Finite-temperature magnetism of disordered Fe-Co alloys

Y. Kakehashi and O. Hosohata
Department of Physics, Hokkaido Institute of Technology, Teine-Maeda, Nishi-ku, Sapporo 006, Japan
(Received 30 May 1989)

The magnetic properties of disordered Fe-Co alloys have been investigated for both bcc and fcc structures using the finite-temperature theory of local-environment effects. The calculated magnetization, Curie temperature, effective Bohr magneton number, Weiss constant, and high-field susceptibility are shown to explain the concentration dependence of the experimental data. It is found that fcc Fe-Co alloys show ferromagnetic instability at 50 at. % Fe and form a spin-glass state after the disappearance of ferromagnetism at $c^*=78$ at. % Fe. This is caused by the nonlinear magnetic coupling between Fe local moments and the local-environment effect on the amplitudes of Fe local moments. Strong local-environment effects around c^* are examined in detail with a prediction of the internal-field distribution for ^{57}Fe.

I. INTRODUCTION

The magnetism of 3*d* transition-metal alloys has been an important problem for understanding itinerant-electron magnetism. Much theoretical effort has been spent on the ground-state properties,[1-11] in particular, the Slater-Pauling curves. The coherent-potential approximation[3,4,8,9] (CPA) was useful in explaining overall features of the ground-state magnetism. Nowadays the basic problems have been solved except for the competing systems such as Fe-Ni and Ni-Mn alloys, in which it is indispensable to determine the local-moment (LM) configurations self-consistently.

On the other hand, the finite-temperature properties contain a wealth of physics because of a variety of thermal excitations, which are not yet understood on the basis of the itinerant-electron model. The theoretical investigations have been made with the development of the spin-fluctuation theories.[12] Kakehashi[13] and Hasegawa[14] extended to the alloy systems the single-site spin-fluctuation theory developed by Cyrot,[15] Hubbard,[16] and Hasegawa.[17] They discussed the finite-temperature magnetism of Fe-Ni and Fe-Cr alloys, respectively. Concentration dependence of the Curie temperatures (T_C) and effective Bohr magneton numbers ($m_{\rm eff}$) have been qualitatively explained. Strong disorder effects around the critical concentration of the ferromagnetic instability (e.g., spin-glass state and broad distribution of internal field), however, were not explained by the single-site theory. We therefore developed the finite-temperature theory of the local-environment effect (LEE) going beyond the single-site theory.[18-22] The theory self-consistently takes into account the LM fluctuations with respect to the atomic configuration by combining the method of the distribution function[23,24] with the functional integral technique.[15-17]

In a series of our systematic investigations of the finite-temperature magnetism of 3*d* transition-metal alloys we have applied the theory to the Ni-Mn,[18] Fe-Ni,[19,20] Fe-V,[21] and Fe-Cr alloys.[22] One of the exciting features which we found is that the fcc Fe-Ni alloys show the anomalous nonlinear magnetic couplings between the nearest-neighbor (NN) Fe LM's; Fe LM's with large amplitude show the ferromagnetic couplings, while those with small amplitude show the antiferromagnetic ones. This behavior is characteristic of the systems in the intermediate regime because it is seen in neither strong nor weak magnet. The nonlinear behavior with the LEE on the amplitude of the Fe LM explained the ferromagnetic instability and the formation of the spin glass (SG) in Fe-Ni alloys. We expect the same anomalies based on the nonlinear magnetic couplings in other fcc Fe-base alloys. In this paper we present the results of our theoretical investigations for the finite-temperature magnetism in the bcc and fcc Fe-Co alloys.

Experimentally it is well known that the fcc Fe-Co alloys are not stable at low temperatures; the bcc lattice is stable between 30 and 100 at. % Fe, and the hcp lattice between 0 and 30 at. % Fe (Ref. 25). Nevertheless much effort has been made to realize the fcc Fe-Co alloys, because they were expected to show anomalous magnetic properties.

Fujimori and Saito[26] stabilized the fcc structure by adding Cr. They investigated the magnetic properties of fcc $(Fe_cCo_{1-c})_{89}Cr_{11}$ $(0.1<c<0.45)$ alloys, and found that the alloys show the Invar anomaly around $c=40$ at. % Fe. The magnetization curve shows a maximum at $c=40$ at. % Fe. The critical concentration of the disappearance of ferromagnetism (c^*) was estimated to be 52 at. % Fe by extrapolating the magnetization versus concentration curve as well as the Curie temperature versus concentration curve.

Nakamura *et al.*[27] investigated the magnetic properties of fcc Fe-Co particles precipitated in a Cu matrix. They found that the magnetization shows a maximum around 45 at. % Fe, and there exists a sharp change at 65 at. % Fe from the ferromagnetic state with large LM's to antiferromagnetic state with small LM's, and both states coexist around there. Recently Tsunoda[28] studied the dilute fcc $Fe_{100-x}Co_x$ $(x<4)$ alloys precipitated in Cu by

using the neutron as well as x-ray diffraction. He found the spin-density wave (SDW) propagating along the cubic b axis with the wavelength of about ten times the lattice spacing although the alloys show basically the first kind antiferromagnetic structure with the wave vector $\mathbf{Q}=(2\pi/a,0,0)$, a being the lattice constant.

By comparing our theoretical results with the experimental data mentioned above, we clarify the magnetic properties of the fcc Fe-Co alloys. In the following section we review the finite-temperature theory of LEE used in our investigations. Section III consists of four subsections concerning the numerical results. We first present the calculated magnetic phase diagram showing the disappearance of the ferromagnetism and existence of SG in the fcc structure. The mechanism of formation of the SG is presented there. In Sec. III B calculated magnetization versus concentration curves are discussed for both bcc and fcc structures. The LEE are shown to play an important role in explaining the anomalies around c^*. The temperature variation of LM's in various local environments and the internal-field distribution functions for ^{57}Fe are presented in Sec. III C. In Sec. III D paramagnetic susceptibility as well as high-field susceptibility are compared with the experimental data. Our results are summarized in Sec. IV with the emphasis on the difference in magnetic properties between the bcc and fcc Fe-Co alloys, and between the Fe-Co and Fe-Ni alloys.

II. METHOD OF CALCULATIONS

We explain in this section an outline of the finite-temperature theory of local-environment effect[19–22] used in the present investigations.

We start from the degenerate-band Hubbard model with Hund's rule coupling, and apply the two-field functional integral method[29] to take into account thermal spin fluctuations within the static approximation. The method transforms the interacting Hamiltonian into a one-electron Hamiltonian H_0 with random exchange fields $\{\xi_i\}$ acting on each site i. Then the local moment on site 0 ($\langle m_0\rangle$) is given by a classical average of the field variable ξ_0 with respect to the energy functional $E(\xi)$ which consists of the free energy for the one-electron Hamiltonian H_0 and the Gaussian terms concerning the field variables.

Next we introduce into the diagonal part of H_0 in $E(\xi)$ an effective medium $\{\mathcal{L}_\sigma^{-1}\}$ which describes the effects of random potentials and the thermal spin fluctuations. When we expand the remaining term in $E(\xi)$ with respect to the site, we take into account the single-site terms $\sum_i E_i(\xi)$ and pair terms $\sum_{(ij)}\Phi_{ij}(\xi_i,\xi_j)$, and neglect higher-order terms. Here $E_i(\xi)$ is an energy functional for the "impurity" on site i embedded in the effective medium and $\Phi_{ij}(\xi_i,\xi_j)$ is the pair-energy functional between sites i and j [see Eq. (2.13) in Ref. 22]. Furthermore we only take into account the nearest-neighbor pair interactions, and neglect those between more distant atoms.

By making use of the decoupling approximation for the surrounding field variables, which is correct up to the second moment, and adopting the molecular field approximation for the surrounding LM's we obtain an expression for $\langle m_0\rangle$ as follows [see Eqs. (2.24) and (2.25) in Ref. 22]:

$$\langle m_0\rangle(\{\gamma_i\},\{\langle m_i\rangle\},=\frac{\int d\xi\,\xi e^{-\beta\Psi(\xi)}}{\int d\xi\, e^{-\beta\Psi(\xi)}}\ , \tag{2.1}$$

$$\Psi(\xi)=E_0(\xi)+\sum_{i\neq 0}^{z}\overline{\Phi}_{0i}(\xi)-\sum_{i\neq 0}^{z}\Phi_{0i}^{\mathrm{ex}}(\xi)\frac{\langle m_i\rangle}{x_i}\ . \tag{2.2}$$

Here γ_i denotes the type of atom on a surrounding site i, and β denotes the inverse temperature, z being the number of the nearest neighbors. $\langle m_i\rangle$ in Eq. (2.2) is the average LM on the neighboring site i. A single-site amplitude x_i is defined by

$$x_i^2=\frac{\int d\xi\,\xi^2 e^{-\beta E_i(\xi)}}{\int d\xi\, e^{-\beta E_i(\xi)}}\ . \tag{2.3}$$

The atomic and exchange pair-energy functional $\overline{\Phi}_{0i}(\xi)$ and $\Phi_{0i}^{\mathrm{ex}}(\xi)$ are defined by

$$\overline{\Phi}_{0i}(\xi)=\tfrac{1}{2}\sum_{\nu=\pm}\Phi_{0i}(\xi,\nu x_i)\ , \tag{2.4}$$

$$\Phi_{0i}^{\mathrm{ex}}(\xi)=-\tfrac{1}{2}\sum_{\nu=\pm}\nu\Phi_{0i}(\xi,\nu x_i)\ . \tag{2.5}$$

Equation (2.1) shows that the central LM in an effective medium is determined by the surrounding atomic and magnetic configurations $\{\gamma_i\}$ and $\{\langle m_i\rangle\}$ via the energy functional $\Psi(\xi)$. The LM's $\{\langle m_i\rangle\}$ should be determined in principle by solving coupled equations of the type (2.1) obtained on each site.

In disordered alloys the random configuration of surrounding atoms produces a local-moment distribution $g_\alpha^{(1)}(m)$ at the central site. Here α denotes the type of atom at the central site. Since the same distribution is expected for the surrounding LM's $\{\langle m_i\rangle\}$, we obtain an integral equation for $g_\alpha^{(1)}(m)$ via Eq. (2.1) [see Eq. (2.26) in Ref. 22]. Further approximations lead to the self-consistent equations for the average LM of the atom α ($[\langle m_\alpha\rangle]_c$) and the configurational average of the square of the LM ($[\langle m_\alpha\rangle^2]_c$):

$$\begin{bmatrix}[\langle m_\alpha\rangle]_c\\ [\langle m_\alpha\rangle^2]_c\end{bmatrix}=\sum_{n=0}^{z}\Gamma(n,z,p_a^{\alpha\alpha})\times\sum_{k=0}^{n}\sum_{l=0}^{z-n}\Gamma(k,n,q_{\alpha+})\times\Gamma(l,z-n,q_{\bar{\alpha}+})\times\begin{bmatrix}\langle\xi_\alpha\rangle_{nkl}\\ \langle\xi_\alpha\rangle_{nkl}^2\end{bmatrix}\ , \tag{2.6}$$

$$q_{\alpha+}=\frac{1}{2}\left[1+\frac{[\langle m_\alpha\rangle]_c}{[\langle m_\alpha\rangle^2]_c^{1/2}}\right]\ , \tag{2.7}$$

$$\langle\xi_\alpha\rangle_{nkl}=\int p_{\alpha nkl}(\xi)\xi\,d\xi\ , \tag{2.8}$$

$$p_{\alpha nkl}(\xi)=\frac{e^{-\beta\Psi_{\alpha nkl}(\xi)}}{\int d\xi\, e^{-\beta\Psi_{\alpha nkl}(\xi)}}\ , \tag{2.9}$$

$$\Psi_{\alpha nkl}(\xi)=E_\alpha(\xi)+n\bar{\Phi}_{\alpha\alpha}(\xi)+(z-n)\bar{\Phi}_{\alpha\bar{\alpha}}(\xi) -(2k-n)\Phi^{\rm ex}_{\alpha\alpha}(\xi)\frac{[\langle m_\alpha\rangle^2]_c^{1/2}}{x_\alpha} -(2l-z+n)\Phi^{\rm ex}_{\alpha\bar{\alpha}}(\xi)\frac{[\langle m_{\bar{\alpha}}\rangle^2]_c^{1/2}}{x_{\bar{\alpha}}}\ . \tag{2.10}$$

Here $\langle\ \rangle$ ($[\ ]_c$) denotes the thermal (configurational) average. The site indices i in x_i and energy functionals have been replaced by the type of atom on site i. $\Gamma(n,z,p_a^{\alpha\alpha})$ in Eq. (2.6) is the binomial distribution function associated with the NN atomic configuration, which is defined by $[z!/n!(z-n)!](p_a^{\alpha\alpha})^n(1-p_a^{\alpha\alpha})^{z-n}$. Here $p_a^{\alpha\alpha}$ is the probability of finding an atom α at a neighboring site of an atom α, and is given in terms of Cowley's atomic short-range order parameter[30] τ as $p_a^{\alpha\alpha}=c_\alpha+(1-c_\alpha)\tau$, c_α being the concentration of atom α.

The binomial distribution functions $\Gamma(k,n,q_{\alpha+})$ and $\Gamma(l,z-n,q_{\bar{\alpha}+})$ in Eq. (2.6) express the fictitious-spin configurations under a given atomic configuration. Here $q_{\alpha+}$ defined by Eq. (2.7) is the probability that the fictitious spin on atom α with magnitude $[\langle m_\alpha\rangle^2]_c^{1/2}$ is in the up direction. $\langle\xi_\alpha\rangle_{nkl}$ is the LM of an atom of type α at the central site when k of the fictitious spins among the surrounding n atoms of type α point up, and l spins of the remaining $z-n$ atoms of type $\bar{\alpha}$ also point up.

Energy functional $\Psi_{\alpha nkl}(\xi)$ in Eq. (2.10) can be calculated when the effective medium $\mathcal{L}_\sigma^{-1}$ is given. The latter is obtained by solving the equation for the coherent-potential approximation under given $[\langle m_\alpha\rangle]_c$ and $[\langle m_\alpha\rangle^2]_c$. Thus the magnetic state is determined by solving both Eq. (2.6) and CPA equation self-consistently. Note that present theory takes into account a large number of surrounding atomic and magnetic configurations ($2^z\times 2^z=16\,771\,216$ for the fcc lattice) in a self-consistent way.

The average amplitude of LM is calculated from the following formula [see Eq. (3.22) in Ref. 29]:

$$[\langle m_\alpha^2\rangle]_c=3n_\alpha-\tfrac{3}{10}n_\alpha^2+\frac{11}{10}\left[[\langle\xi_\alpha^2\rangle]_c-\frac{2}{\beta\tilde{J}_\alpha}\right], \tag{2.11}$$

$$[\langle\xi_\alpha^2\rangle]_c=\sum_{n=0}^{z}\Gamma(n,z,p_a^{\alpha\alpha})\times\sum_{k=0}^{n}\sum_{l=0}^{z-n}\Gamma(k,n,q_{\alpha+})\times\Gamma(l,z-n,q_{\bar{\alpha}+})\langle\xi_\alpha^2\rangle_{nkl}\ , \tag{2.12}$$

$$\langle\xi_\alpha^2\rangle_{nkl}=\int\xi^2 p_{\alpha nkl}(\xi)d\xi\ . \tag{2.13}$$

Here n_α denotes the d electron number for the atom α and $\tilde{J}_\alpha$ is an effective exchange energy parameter for atom α. The distribution of the LM on atom α and the internal-field distribution affecting the nucleus of atom α are obtained from the following expressions (see Appendix in Ref. 21):

$$\begin{bmatrix} g_\alpha^{(1)}(M)\\ P_\alpha(H)\end{bmatrix}=\sum_{n=0}^{z}\Gamma(n,z,p_a^{\alpha\alpha})\sum_{k=0}^{n}\sum_{l=0}^{z-n}\Gamma(k,n,q_{\alpha+})\Gamma(l,z-n,q_{\bar{\alpha}+})\begin{bmatrix}\delta(M-\langle\xi_\alpha\rangle_{nkl})\\ \delta(H-H_{\alpha nkl})\end{bmatrix}. \tag{2.14}$$

Here

$$H_{\alpha nkl}=a_\alpha\langle\xi_\alpha\rangle_{nkl}+(2k-1)b_{\alpha\alpha}[\langle m_\alpha\rangle^2]_c^{1/2} +(2l-z+n)b_{\alpha\bar{\alpha}}[\langle m_{\bar{\alpha}}\rangle^2]_c^{1/2}\ . \tag{2.15}$$

We have assumed here a phenomenological expression for the internal field acting on atom i,

$$H_i=a_i\langle m_i\rangle+\sum_{j=1}^{z}b_{ij}\langle m_j\rangle\ , \tag{2.16}$$

where $\langle m_j\rangle$ is a local moment at the neighboring site j. Recently Ebert *et al.*[31] have shown that the contribution to the Fermi contact hyperfine field due to core polarization is described by the first term at the right-hand side of Eq. (2.16), while the result for the contribution of the conduction band suggests that one needs the second terms in the phenomenological expression (2.16).

III. NUMERICAL RESULTS

A. Magnetic phase diagram

The numerical calculations have been performed by using the following set of input parameters:

$$n_{\rm Fe}=7.0,\quad W_{\rm Fe}=0.450\ {\rm Ry},\quad \tilde{J}_{\rm Fe}=0.070\ {\rm Ry}\ ,$$
$$n_{\rm Co}=8.0,\quad W_{\rm Co}=0.441\ {\rm Ry},\quad \tilde{J}_{\rm Co}=0.105\ {\rm Ry}\ .$$

Here n_α, W_α, and $\tilde{J}_\alpha$ are the d electron number, d-band width, and effective exchange energy parameter, respectively. These parameters lead to the observed magnetizations $2.216\mu_B$ (Ref. 32) for the bcc Fe and $1.74\mu_B$ (Ref. 33) for fcc Co at $T=0$. In the calculation for the fcc alloys we adopted $n_{\rm Fe}=7.05$, which was found to give better critical concentration of the ferromagnetic instability in Fe-Ni alloys.[20] The model densities of states for noninteracting systems used in the present calculations are the same as in Fe-Ni alloys. In the following we assume that the alloys show a complete disorder (i.e., $\tau=0$).

Although the present theory is based on a pair approximation the calculated local densities of states (LDOS) at low temperatures reproduce well those calculated by using the cluster CPA method at $T=0$ (Ref. 6) as shown in Fig. 1. This agreement has also been found in Fe-V (Ref. 21) and Fe-Ni alloys,[20] establishing the validity of the present theory in the concentrated alloys.

A magnetic phase diagram for Fe-Co alloys is given in

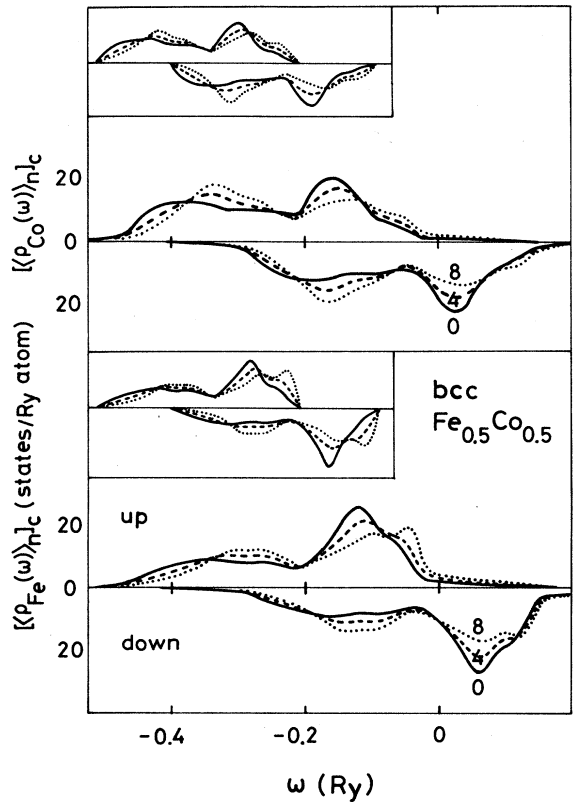

FIG. 1. Average local densities of states at $T=150$ K for the bcc $Fe_{0.5}Co_{0.5}$ alloy in various environments. Here and in the following figures the local environments are specified by the number of Fe nearest neighbors (n). The insets show the ground-state results based on the cluster CPA (Ref. 6).

Fig. 2. The calculated Curie temperature for fcc Co is 3160 K, which is twice as large as the observed value (1400 K). This is partly due to the single-site approximation for the thermal average, which completely neglects the magnetic short-range order, and partly due to the choice of the parameter $\tilde{J}_{Co}$. Note that we chose $\tilde{J}_{Co}$ so that the calculated ground-state magnetization agrees with the observed one ($1.74\mu_B$).[33] The orbital contribution to the ground-state magnetization is very large in the case of Co ($=0.14\ \mu_B$). Calculated T_C becomes 2500 K if we choose $\tilde{J}_{Co}$ so as to reproduce the spin contribution ($1.60\mu_B$) (Ref. 34) at $T=0$.

Curie temperatures in the bcc lattice decrease as Fe concentration increases, those in the fcc decrease more rapidly with increasing Fe concentration. This trend is consistent with the experimental data shown in the inset of Fig. 2. We found that the ferromagnetism disappears at $c^*=78$ at. % Fe. This value of c^* is in good agreement with that expected from the experimental inverse susceptibilities at high temperatures (see Sec. III D). The extrapolated value of c^* in the fcc $(Fe_cCo_{1-c})_{89}Cr_{11}$ alloys is 52 at. % Fe (Ref. 26). The critical concentration for the fcc Fe-Co alloy particles precipitated in a Cu matrix is reported to be $c^*=90$ at. % Fe (Ref. 27). Theoretical value is between the two.

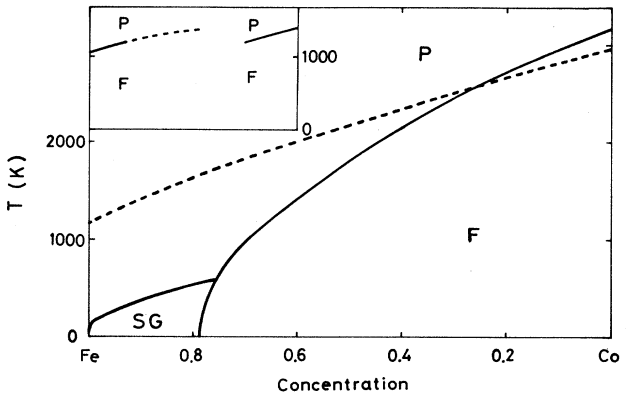

FIG. 2. Calculated magnetic phase diagram for the bcc (dashed curve) and fcc (solid curves) Fe-Co alloys showing the ferromagnetic (F), paramagnetic (P), and spin-glass (SG) states. The inset shows the experimental result (Ref. 37), in which the extrapolated Curie temperatures in the bcc structure are shown by the dashed curve.

The calculated SG temperatures (~ 500 K) are certainly overestimated because of the neglect of the frustration effect of spins on the fcc lattice. We expect that the real T_g are less than 100 K, assuming that the reduction of T_g is the same as in Fe-Ni alloys.[20]

The origin of the SG is the same as in Fe-Ni alloys. In Fig. 3 we show the effective exchange coupling $\mathcal{J}_{\alpha\gamma}$ between the NN LM's α and γ with average amplitudes. The coupling $\mathcal{J}_{FeFe}$ in the fcc lattice changes the sign at 55 at. % Fe with increasing Fe concentration, and becomes approximately zero in the SG regime. Other couplings $\mathcal{J}_{CoCo}$ and $\mathcal{J}_{CoFe}$ are positive. Thus the formation of the SG solution is not explained by a simple localized model. In Fig. 4 we present the atomic and exchange pair-energy functionals $\bar{\Phi}_{Fe\gamma}(\xi)$ and $\Phi^{ex}_{Fe\gamma}(\xi)$ ($\gamma=$Fe or

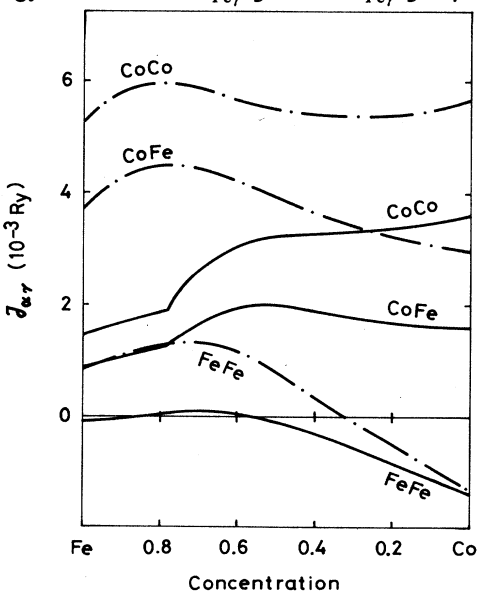

FIG. 3. Effective exchange pair interactions $\mathcal{J}_{\alpha\gamma}$ for bcc (dotted-dashed curves) and fcc (solid curves) structures at 150 K.

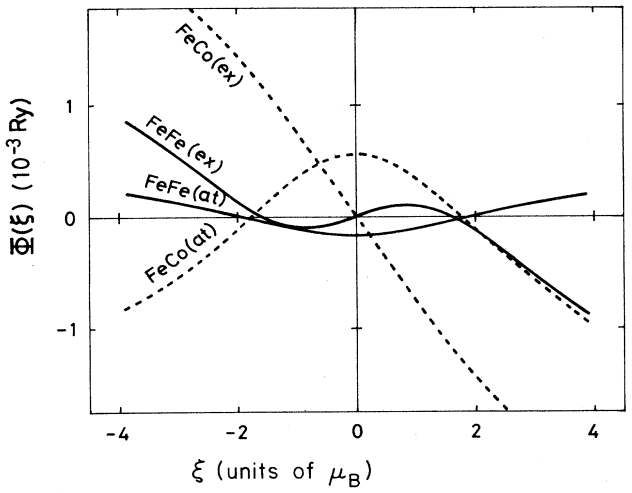

FIG. 4. Pair-energy functionals $\bar{\Phi}_{\alpha\gamma}(\xi)$ [$\alpha\gamma$(at)] and $-\Phi^{ex}_{\alpha\gamma}(\xi)$ [$\alpha\gamma$(ex)] for the central Fe local moment (α=Fe) in the fcc $Fe_{0.8}Co_{0.2}$ alloy at T=150 K.

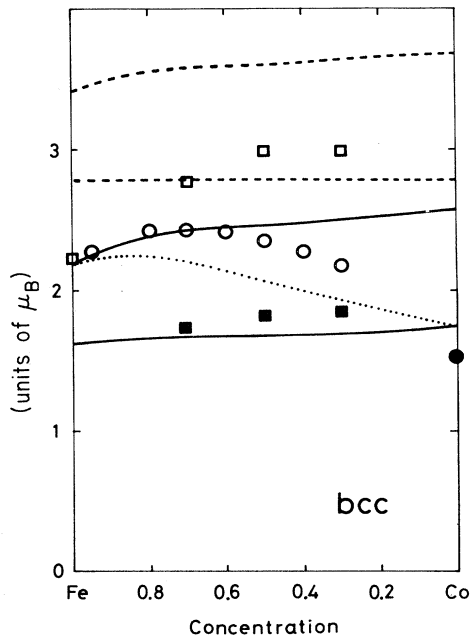

FIG. 5. Concentration dependence of various local moments (LM) for the bcc structure at T=150 K. · · · ·, magnetization. ——, $[\langle m_\alpha \rangle]_c$. — — —, $[\langle m_\alpha^2 \rangle]_c^{1/2}$. Experimental data of the ground-state magnetization are shown by ○ (Ref. 38) and ● (Ref. 39). Experimental $[\langle m_\alpha \rangle]_c$ are shown by □ (α=Fe) and ■ (α=Co) (Ref. 40).

Co), which means the pair-energy gain of a flexible central Fe LM ξ when the neighboring LM with the amplitude x_γ points up [see Eq. (2.2)]. The exchange energy functional $\Phi^{ex}_{FeFe}(\xi)$ shows and S-shaped curve as seen in Fe-Ni alloys. This means that the Fe LM's with the amplitude ($\langle \xi_\alpha^2 \rangle^{1/2}$) less (more) than about 1.7μ_B couple antiferromagnetically (ferromagnetically) to the neighboring Fe LM. Since various atomic configurations on the surrounding sites produce the various amplitudes of Fe LM's via the atomic pair-energy functionals $\bar{\Phi}_{\alpha\gamma}(\xi)$, the ferro- and antiferromagnetic couplings between Fe LM's appear in the disordered alloys. This produces the SG solution.

We have not yet investigated the stability of the antiferromagnetic state because of laborious calculations. It is probable that a long-range magnetic order with type-I antiferromagnetism becomes more stable than the SG when the Fe concentration is increased further after disappearance of ferromagnetism. In particular, the dumping effect[35] on the magnitude of pair interactions with increasing atomic distance becomes less important. A long-range interaction, which we did not take into account in the present calculations, is then expected to develop at more than 90 at. % Fe. It is important for understanding the SDW in dilute Fe_cCo_{1-c} ($c>0.95$) alloys.[28]

B. Magnetic moments and ferromagnetic instability

The ground-state magnetization of the bcc Fe-Co alloys is well known to show the maximum at 30 at. % Co, and then decrease as the Co concentration increases. This behavior has been explained by using the rigid band model,[1,7,36] CPA,[4] and superlattice approach.[11] Present results shown in Fig. 5 explain the experimental data. The maximum is well known to be explained by the rapid increase of Fe LM's due to a band filling of up-spin electrons and the saturation at about 40 at. % Co.

The amplitude of LM's ($[\langle m_\alpha^2 \rangle]_c^{1/2}$) is about 1.5 times as large as the local magnetization $[\langle m_\alpha \rangle]_c$ because of the quantum effect as shown in Fig. 5, but the concentration dependence is similar to $[\langle m_\alpha \rangle]_c$ since there is no directional spin disorder.

The LM's in various environments on the bcc lattice are shown in Fig. 6. The calculated results, which are in good agreement with the previous results based on the cluster CPA,[6] show considerable LEE on the Fe LM because of the existence of holes in the up-spin band, and small change of the Co LM due to the strong ferromagnetism.

New results obtained here are the behavior in the regime $c_{Fe}<30$ at. % Fe and the LEE on the amplitudes of the LM's. The latter shows large amplitude fluctuations in Fe LM's. In the former we find that the LEE on the Fe LM again becomes large at $c_{Fe}<20$ at. % Fe. This is related to the antiferromagnetic coupling $\mathcal{J}_{FeFe}$ in the regime $c_{Fe}<30$ at. % Fe (see Fig. 3). It is worthwhile to point out that the strong LEE such as the reversal of Fe LM is not seen in the bcc alloys. This is the reason the superlattice approach,[11] in which the alloys are simulated by a superlattice with the same composition, has been successful in reproducing the bulk magnetizations in the bcc Fe-Co alloys.

The fcc Fe-Co alloys, on the other hand, show anomalous concentration dependence of magnetization as shown in Fig. 7. The magnetization curve shows the ferromagnetic instability at about 50 at. % Fe. This instability is a feature inherent in the close-packed Fe alloys as

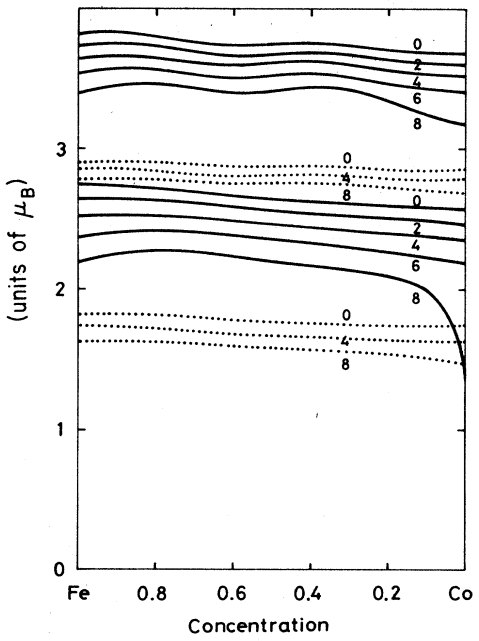

FIG. 6. Average LM ($[\langle m_\alpha \rangle_n]_c$) and the amplitude ($[\langle m_\alpha^2 \rangle_n]_c^{1/2}$) for Fe (solid curves) and Co (dotted curves) in various environments (n) at $T=150$ K in the bcc Fe_cCo_{1-c} alloys.

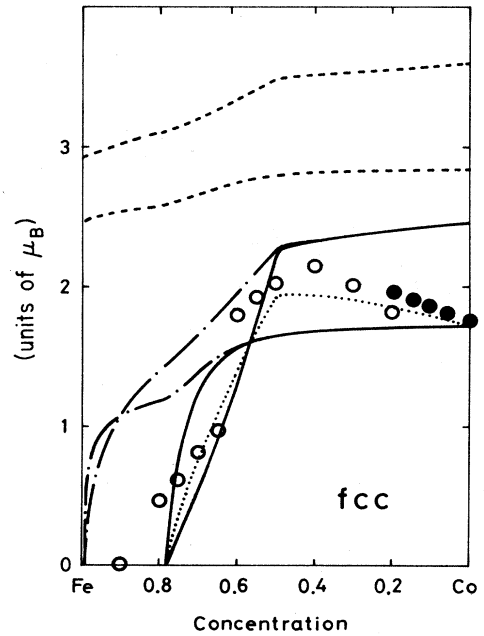

FIG. 7. Concentration dependence of LM's for the fcc structure at $T=150$ K. · · · ·, magnetization. ——, $[\langle m_\alpha \rangle]_c$. — ·—, $[\langle m_\alpha \rangle^2]_c^{1/2}$. — — —, $[\langle m_\alpha^2 \rangle]_c^{1/2}$. Experimental data for the bulk magnetization are shown by solid circles (Ref. 41), while the data for the fcc Fe-Co particles precipitated in a Cu matrix are shown by open circles (Ref. 27).

discussed in our previous paper for Fe-Ni alloys.[20] However, the slope of the decreasing magnetization curve is not so steep when compared with that in Fe-Ni alloys; we need more than 25 at. % Fe change in Fe-Co alloys from the beginning of the instability to the disappearance of the ferromagnetism, while it is about 10 at. % Fe in Fe-Ni alloys. This is because the average d electron number in Fe-Ni alloys changes with increasing Fe concentration twice as fast as that in Fe-Co alloys, and because Co atoms have well-defined LM when compared with Ni atoms in alloys.

The theory seems to explain qualitatively the experimental magnetization versus concentration curve deduced from the fcc Fe-Co precipitated particles. However, our magnetization curve continuously changes, while the experimental data suggest a sudden change at 65 at. % Fe. It reminds us of the transition from the high-spin to the low-spin state which has recently been found in the band calculations.[42,43] The Mössbauer data are, however, interpreted as a sharp transition from the ferro- to the antiferromagnetism with small moment. We have to take the following facts into consideration in comparison with the theoretical results. First, the bcc and fcc structures coexist in the Fe-Co precipitated particles. This coexistence might influence the bulk magnetic state. Second, the effect of atomic short-range order on the magnetization around c^* has not yet been examined both experimentally and theoretically.

The Fe and Co LM's show a strong LEE in the instability range between 50 at. % Fe and 80 at. % Fe as shown in Fig. 8. The strong disturbance of LM's is explained as follows. The pair energy $\bar{\Phi}_{FeCo}(\xi)$ $[\bar{\Phi}_{FeFe}(\xi)]$ acts to extend (shrink) the amplitude $\langle \xi_{Fe}^2 \rangle^{1/2}$ at the central site (see Fig. 4). Thus the amplitude $\langle \xi_{Fe}^2 \rangle^{1/2}$ de-

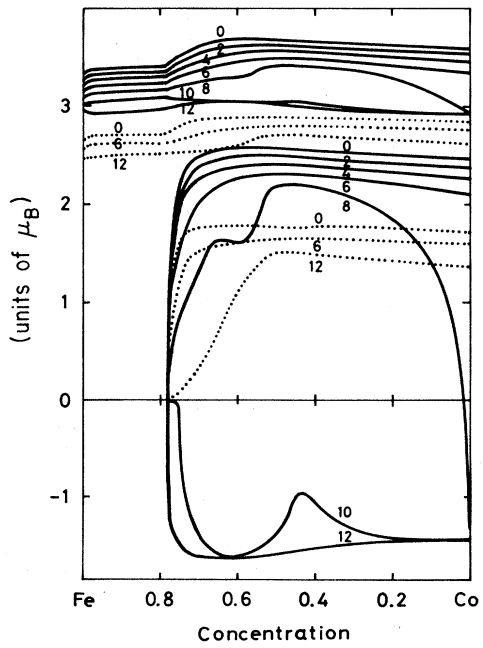

FIG. 8. The same as in Fig. 6 but for the fcc alloys.

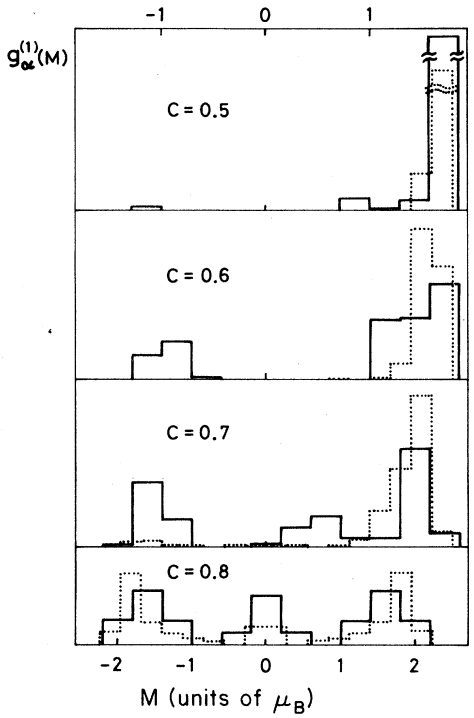

FIG. 9. Distribution functions for Fe (solid curves) and Co (dotted curves) LM's in the fcc Fe_cCo_{1-c} alloys at $T=150$ K. The upper (lower) scale of M is for Co (Fe) LM's.

creases with increasing Fe concentration. In particular, when the amplitudes of Fe LM's with eight Fe NN's become smaller than about $2\mu_B$, the Fe LM's become unstable because of the nonlinear coupling $\Phi^{ex}_{FeFe}(\xi)$. Feedback of the new configuration to the effective medium drives the rapid decrease of the magnetization, leading to the disappearance of the ferromagnetism at about $c^*=78$ at. % Fe. The SG state appears after the disappearance since the instability of the ferromagnetism is accompanied by the competition of the ferro- and antiferromagnetic couplings between Fe LM's. (Note that $[\langle m_\alpha\rangle^2]_c^{1/2}$ remains nonzero at $c>c^*$ in Fig. 7.)

The LM distribution functions are given in Fig. 9 as a function of Fe concentration. As the magnetization decreases near the critical concentration c^* a peak at $M=-1.2\mu_B$ develops first in $g^{(1)}_{Fe}(M)$, and later a peak at $M=-1.3\mu_B$ appears in $g^{(1)}_{Co}(M)$. This behavior implies that the ferromagnetic instability is driven by the antiferromagnetic couplings between Fe LM's. The distribution $g^{(1)}_{Co}(M)$ at $c_{Fe}=0.8$ has double peaks at $M=\pm1.3\mu_B$ since Co atoms have well-defined LM's. This is qualitatively different from $g^{(1)}_{Ni}(M)$ in Fe-Ni alloys[20] which shows a single peak around $M=0$ near c^*.

C. Temperature variation of local magnetic moments

The magnetization versus temperature curves are presented in Fig. 10. It is seen that the curves at 60 at. % Fe in the fcc structure deviate downwards from the Brillouin curve. This is understood as the effect of the ran-

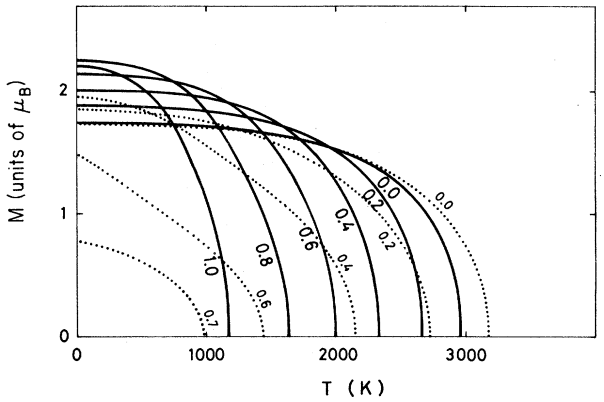

FIG. 10. Magnetization vs temperature curves for various concentrations in the bcc (solid curves) and fcc (dotted curves) Fe_cCo_{1-c} alloys.

domness and the characteristics of the temperature-induced weak ferromagnetism. In the present case the former origin should be dominant because the Fe and Co LM's in Fe-Co alloys show more localized character than in the Fe-Ni alloys.[19]

Figure 11 shows a typical example of the temperature variations of the LM's in various local environments near c^*. The Fe atoms with about eight Fe NN's rapidly lose their average LM's because of the weak local molecular fields caused by surrounding Fe and Co LM's. The reversal of Fe LM's with increasing temperature which was found in Fe-Ni alloys[19-20] is not seen in the present case. This is because the amplitudes of Fe LM's are not so

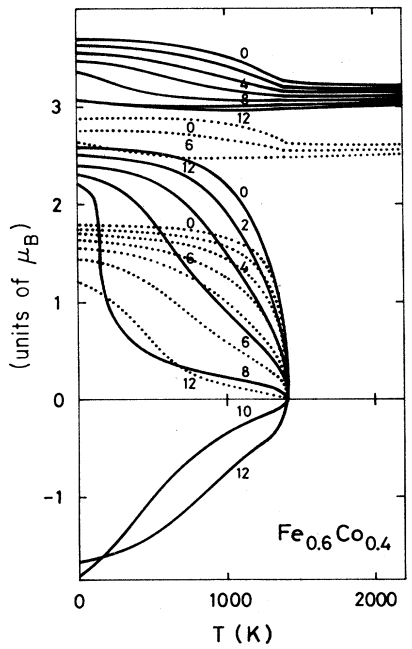

FIG. 11. Temperature dependence of the average LM ($[\langle m_\alpha\rangle_n]_c$) and amplitudes ($[\langle m_\alpha^2\rangle_n]_c$) for Fe (solid curves) and Co (dotted curves) atoms in various environments on the fcc lattice.

strongly reduced with increasing temperature, so that the nonlinear coupling between Fe LM's does not change the sign.

The temperature variations of the distribution functions for the fcc structure are shown in Fig. 12 for 70 at. % Fe. In the fcc structure the average Fe LM $[\langle m_{\mathrm{Fe}} \rangle]_c$ is only $0.75\mu_B$ at $0.31T_C$, but $g^{(1)}_{\mathrm{Fe}}(M)$ shows a broad distribution. The latter shrinks gradually with increasing temperature and merges into a central peak at $M=0$ above T_C. On the other hand, the Co LM's at $T=0.31T_C$ show a single peak at $M=1.5\mu_B$, indicating the strong ferromagnetic character. But, at higher temperatures the Co LM's also show a broad distribution. This is different from the behavior of Ni LM's in Fe-Ni alloys, in which Ni LM's are hardly influenced by the local environment at finite temperatures.

A LM distribution leads to an internal-field distribution $P_\alpha(H)$ according to Eq. (2.16). Theoretical $P_{\mathrm{Fe}}(H)$ are presented for 60 and 70 at. % Fe in Fig. 13. The distributions have two well-defined peaks corresponding to parallel and antiparallel Fe LM's at low temperatures. This trend is seen in the Mössbauer experiment by Nakamura *et al.*[27] When the temperature is elevated the valley between the two peaks is filled up by the Fe LM's with eight and nine NN Fe LM's. Single-peak structure of the distribution appears above $T_1 \approx 0.65T_C$. Note that this value is smaller than $T_1 \approx 0.90T_C$ in $Fe_{0.6}Ni_{0.4}$ alloys.

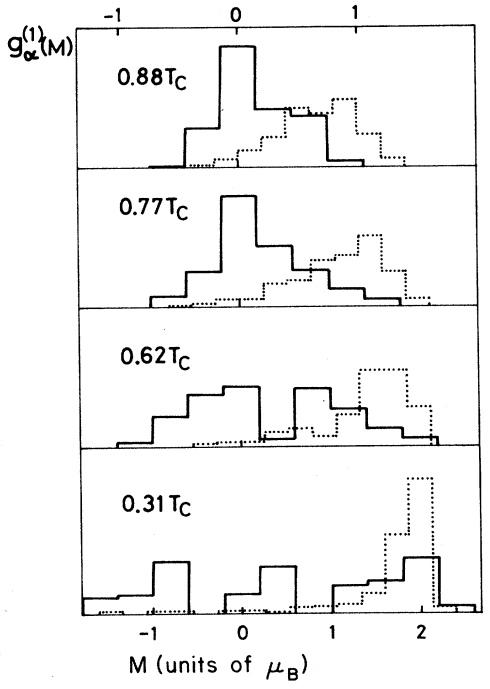

FIG. 12. Temperature variation of the distribution functions for Fe (solid curves with the lower scale for M) and Co (dotted curves with the upper scale for M) LM's in the fcc $Fe_{0.7}Co_{0.3}$ alloys.

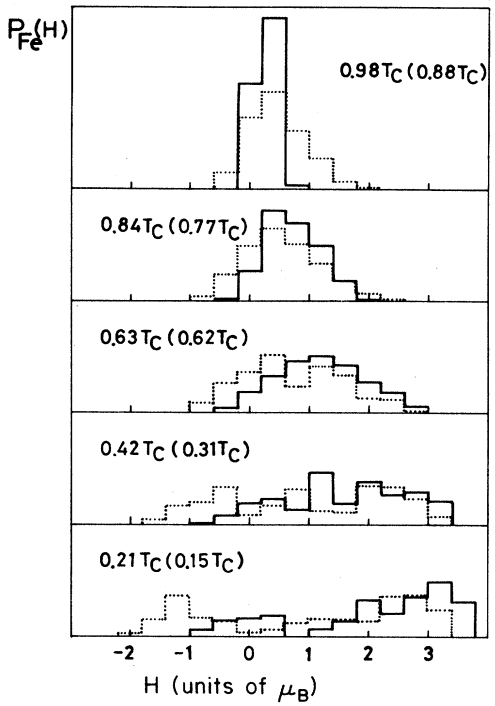

FIG. 13. Temperature variation of the calculated internal-field distribution functions in units of $a_{\mathrm{Fe}}=1$ for ^{57}Fe at 60 at. % Fe (solid curves) and 70 at. % Fe (dotted curves). The temperatures in the parentheses are for 70 at. % Fe alloys. The parameters $b_{\mathrm{FeFe}}/a_{\mathrm{Fe}}=b_{\mathrm{FeCo}}/a_{\mathrm{Fe}}=0.06$ which have been used in Fe-Ni alloys are adopted (Ref. 20).

D. Susceptibility

The paramagnetic susceptibilities in the fcc lattice are directly compared with the experimental data at high temperatures. Calculated results are shown in Fig. 14. The susceptibilities show a cusp at T_g and follow the Curie-Weiss law at high temperatures. Calculated effective Bohr magneton number (m_{eff}) and the Weiss constant (Θ_p) are compared with the experimental data in Fig. 15. The Weiss constants in the fcc structure decrease with increasing Fe concentration and change the sign at 75 at. % Fe. This value is in good agreement with the experimental value 70 at. % Fe. The calculated effective Bohr magneton numbers also qualitatively agree with the experimental results. The increase of m_{eff} in the fcc structure is due to the gradual change from the strong to the weak ferromagnetism with increasing Fe concentration.

Concentration dependences of high-field spin susceptibilities at low temperatures are given in Fig. 16. Calculated susceptibilities χ in the bcc explain qualitatively the concentration dependence of the experimental data. Enhancement of χ in the Fe-rich region is due to the formation of holes in the up-spin band. Experimentally the susceptibility in the bcc structure shows a sharp maximum at 86 at. % Fe at room temperatures.[46] This is not explained by the present theory. It might be attributed to the details of the DOS or the dynamical spin fluctuations.

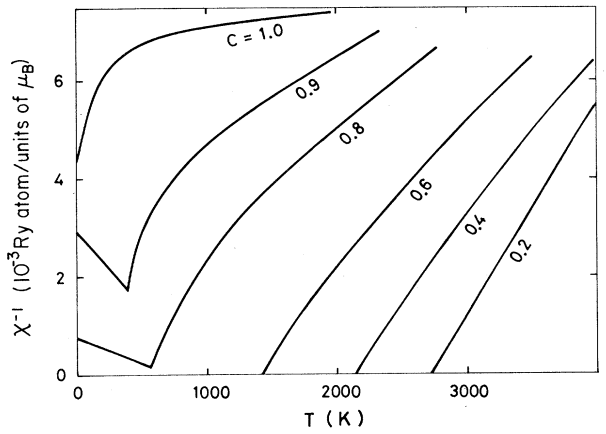

FIG. 14. Paramagnetic inverse spin susceptibility vs temperature curves for the fcc Fe_cCo_{1-c} alloys.

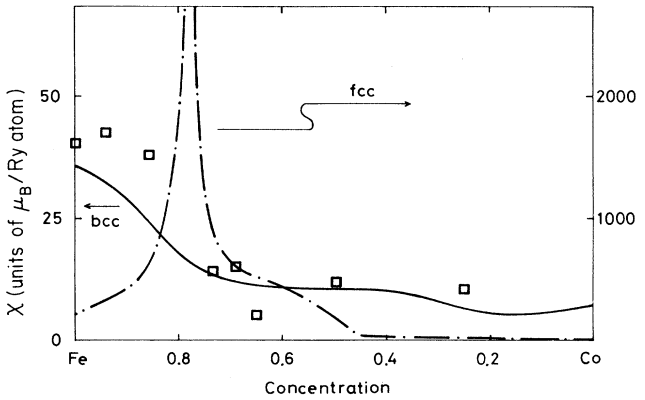

FIG. 16. High-field spin susceptibilities at $T=150$ K for the bcc (solid curve) and fcc (dotted-dashed curve) structures. Experimental data at 4.2 K in the bcc structure are shown by open squares (Ref. 46).

On the other hand, the susceptibility for the fcc structure diverges at c^*. The magnitude in the regime between 50 and 100 at. % Fe is much larger than that in the bcc structure because of the reversal of Fe LM's in the applied magnetic field.

IV. SUMMARY AND DISCUSSION

We have investigated the magnetic properties of Fe-Co alloys at finite temperatures by using the finite-temperature theory of LEE. Concentration dependence of the magnetization, Curie temperature, effective Bohr magneton number, and Weiss constant has been explained qualitatively or semiquantitatively.

The bcc Fe-Co alloys show no strong magnetic disturbance because all the magnetic couplings between constituent atoms are ferromagnetic. The alloying effects under given ferromagnetic arrangement are basically explained by the CPA or superlattice approach. The LEE on the LM's simply produces a width around the average LM's. The width for Fe LM's is larger than that for Co LM's because of the existence of holes in the up-spin band for Fe.

On the other hand, Fe LM's in the fcc lattice have the nonlinear couplings as seen in Fe-Ni. Therefore the fcc Fe-Co alloys show the strong disorder effects due to LEE on the amplitude of Fe LM's in the Fe-rich region. In this case the self-consistent determination of the LM configuration is essential for the description of the magnetism. The calculated magnetic phase diagram shows the disappearance of the ferromagnetism at 78 at. % Fe. We predict the SG state after disappearance of the ferromagnetism. The transition temperatures T_g are expected to be less than 100 K.

Although the mechanism of ferromagnetic instability and SG in the fcc Fe-Co alloys is the same as in the fcc Fe-Ni alloys, we found some characteristics of Fe-Co alloys. (1) The magnetization versus concentration curve decreases less rapidly after occurrence of the ferromagnetic instability. (2) The critical concentration c^* where $T_C=0$ shifts to the γ-Fe side by about 10 at. % as compared with that in Fe-Ni alloys. (3) The Co LM's also show a broad distribution near c^*. (4) The internal-field distribution $P_{Fe}(H)$ around 65 at. % Fe shows a clear two-peak structure at low temperatures, but changes to a single-peak structure above $0.65T_C$ which is lower than $0.90T_C$ in Fe-Ni alloys. These differences are mainly explained by the fact that Co LM's are more localized than Ni LM's.

Apparently many of our conclusions for the fcc Fe-Co alloys have not yet been verified experimentally. In par-

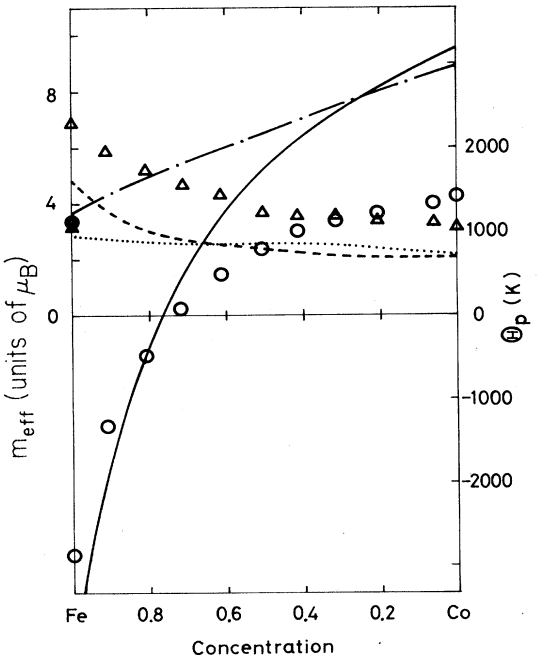

FIG. 15. Concentration dependence of the effective Bohr magneton number m_{eff} [dotted (bcc) and dashed (fcc) curves] and the Weiss constant [dotted-dashed (bcc) and solid (fcc) curves]. Open (solid) triangles and circles show the experimental m_{eff} and Weiss constants, respectively, for the fcc (Ref. 44) (bcc) (Ref. 45) structures.

ticular the magnetic phase diagram in the regime $60 < c < 90$ at. % Fe is not well known. According to the recent phase diagram for dilute fcc Fe_cCo_{1-c} ($c > 0.95$) particles precipitated in Cu,[28] the SDW with a basic structure of type-I antiferromagnetism is expected to disappear around 92 at. % Fe. It has not yet been clarified whether or not the SG appears between 92 at. % Fe and c^*. The second point to be clarified is that our theory predicts a rapid but smooth magnetization versus concentration curve, while the experimental data of the fcc Fe-Co particles suggest a sudden change from the ferro- to antiferromagnetism at 65 at. % Fe. It should be examined whether the latter is intrinsic to the bulk fcc Fe-Co alloys with no atomic short-range order. We hope that novel experimental techniques will solve these problems stabilizing the fcc Fe-Co alloys.

ACKNOWLEDGMENTS

The authors would like to thank Dr. H. Ebert for valuable discussion on a phenomenological expression for hyperfine fields, and Dr. Y. Tsunoda for informing them of the experimental data for the fcc Fe-Co alloys.

[1]J. Friedel, Nuovo Cimento Suppl. **7**, 287 (1958).
[2]P. W. Anderson, Phys. Rev. **124**, 1030 (1961).
[3]P. Soven, Phys. Rev. **156**, 809 (1967).
[4]H. Hasegawa and J. Kanamori, J. Phys. Soc. Jpn. **31**, 382 (1971); **33**, 1599 (1972).
[5]H. Miwa, Prog. Theor. Phys. **52**, 1 (1974); N. Hamada and H. Miwa, Prog. Theor. Phys. **59**, 1045 (1978).
[6]N. Hamada, J. Phys. Soc. Jpn. **46**, 1759 (1979).
[7]J. Kollár, U. K. Poulsen, and O. K. Andersen, in *Proceedings of the VIII Symposium on Electronic Structure of Metals and Alloys,* edited by J. Kollár (Dresden, 1978), p. 29.
[8]D. D. Johnson, F. J. Pinski, and G. M. Stocks, J. Phys. **57**, 3018 (1985).
[9]H. Ebert, H. Winter, B. L. Gyorffy, D. D. Johnson, and F. J. Pinski, J. Phys. F **18**, 719 (1988).
[10]A. R. Williams, V. L. Moruzzi, C. D. Gellatt, Jr., and J. Kubler, J. Magn. Magn. Mater. **31-34**, 88 (1983).
[11]K. Schwarz, P. Mohn, P. Blaha, and J. Kubler, J. Phys. **14**, 2659 (1984).
[12]For a review on recent development, see *Metallic Magnetism,* Vol. 42 of *Topics in Current Physics,* edited by H. Capellmann (Springer-Verlag, Berlin, 1987).
[13]Y. Kakehashi, J. Phys. Soc. Jpn. **49**, 2421 (1980); **50**, 2236 (1981).
[14]H. Hasegawa, J. Phys. Soc. Jpn. **50**, 802 (1981).
[15]M. Cyrot, J. Phys. (Paris) **33**, 125 (1972).
[16]J. Hubbard, Phys. Rev. B **19**, 2626 (1979); **20**, 4584 (1979); **23**, 597 (1981).
[17]H. Hasegawa, J. Phys. Soc. Jpn. **46**, 1504 (1979); **49**, 178 (1980).
[18]Y. Kakehashi, J. Phys. Soc. Jpn. **50**, 3177 (1980); **51**, 94 (1982); **52**, 637 (1983); J. Magn. Magn. Mater. **43**, 79 (1984).
[19]Y. Kakehashi, J. Magn. Magn. Mater. **37**, 189 (1983); **66**, 1163 (1987).
[20]Y. Kakehashi, Phys. Rev. B **38**, 474 (1988).
[21]Y. Kakehashi, Phys. Rev. B **32**, 3035 (1985).
[22]Y. Kakehashi, Phys. Rev. B **35**, 4973 (1987).
[23]F. Matsubara, Prog. Theor. Phys. **52**, 1124 (1974).
[24]S. Katsura, S. Fujiki, and S. Inawashiro, J. Phys. C **12**, 2839 (1979).
[25]See, for example, R. M. Bozorth, *Ferromagnetism* (Van Nostrand, Princeton, 1968).
[26]H. Fujimori and H. Saito, J. Jpn. Inst. Met. **33**, 375 (1969).
[27]Y. Nakamura, M. Shiga, and S. Santa, J. Phys. Soc. Jpn. **26**, 210 (1969); Y. Muraoka, T. Fujiwara, M. Shiga, and Y. Nakamura, J. Phys. Soc. Jpn. **50**, 3284 (1981).
[28]Y. Tsunoda, J. Phys. F **18**, L251 (1988); J. Phys. Soc. Jpn. **58**, 1648 (1989); J. Phys. Cond. Matter (to be published); Y. Tsunoda and N. Kunitomi, J. Phys. F **18**, 1405 (1988).
[29]Y. Kakehashi, Phys. Rev. B **34**, 3243 (1986).
[30]J. M. Cowley, Phys. Rev. **77**, 669 (1950).
[31]H. Ebert, H. Winter, D. D. Johnson, and F. J. Pinski, Hyperfine Interactions **51**, 925 (1989).
[32]H. Danan, A. Herr, and A. J. P. Meyer, J. Appl. Phys. **39**, 669 (1968).
[33]M. J. Besnus, A. J. P. Meyer, and R. Berniger, Phys. Lett. **32**, 192 (1970).
[34]R. A. Reck and D. L. Fry, Phys. Rev. **184**, 492 (1969).
[35]A. Bieber and F. Gautier, Solid State Commun. **39**, 149 (1981); J. Phys. Soc. Jpn. **53**, 2251 (1981).
[36]A. P. Malozemoff, A. R. Williams, and V. L. Moruzzi, Phys. Rev. B **29**, 1620 (1984).
[37]M. Hansen and K. Anderko, *Constitution of Binary Alloys* (McGraw-Hill, New York, 1958).
[38]D. I. Bordos, J. Appl. Phys. **40**, 1371 (1969).
[39]G. A. Prinz, Phys. Rev. Lett. **54**, 1051 (1985).
[40]M. F. Collins and J. B. Forsyth, Philos. Mag. **8**, 401 (1963).
[41]R. M. Bozorth, *Ferromagnetism* (Van Nostrand, Princeton, 1968), p. 441.
[42]D. M. Roy and D. G. Pettifor, J. Phys. F **7**, L183 (1977).
[43]V. L. Moruzzi, Phys. Rev. Lett. **57**, 2211 (1986); V. L. Moruzzi, P. M. Marcus, K. Schwarz, and P. Mohn, Phys. Rev. B **34**, 1784 (1986).
[44]Y. Barnier, R. Pauthenet, and L. Neel, Cobalt No. 21 (1963) (Cobalt Information Center).
[45]M. Fallot, J. Phys. Radium V, 153 (1944).
[46]J. H. M. Stoelinga, R. Gersdorf, and G. de Vries, Physica **41**, 457 (1969).